Role of Orography, Diurnal Cycle, and Intraseasonal Oscillation in Summer Monsoon Rainfall over the Western Ghats and Myanmar Coast

SHOICHI SHIGE, YUKI NAKANO, AND MUNEHISA K. YAMAMOTO

Graduate School of Science, Kyoto University, Kyoto, Japan

(Manuscript received 1 December 2016, in final form 3 August 2017)

ABSTRACT

Rainfall over the coastal regions of western India [Western Ghats (WG)] and Myanmar [Arakan Yoma (AY)], two regions experiencing the heaviest rainfall during the Asian summer monsoon, is examined using a Tropical Rainfall Measuring Mission (TRMM) Precipitation Radar (PR) dataset spanning 16 years. Rainfall maxima are identified on the upslope of the WG and the coastline of AY, in contrast to the offshore locations observed in previous studies. Continuous rain with slight nocturnal and afternoon–evening maxima occurs over the upslope of the WG, while an afternoon peak over the upslope and a morning peak just off the coast are found in AY, resulting in different locations of the rainfall maxima for the WG (upslope) and AY (coastline). Large rainfall amounts with small diurnal amplitudes are observed over the WG and AY under strong environmental flow perpendicular to the coastal mountains, and vice versa. Composite analysis of the boreal summer intraseasonal oscillation (BSISO) shows that the rain anomaly over the WG slopes lags behind the northward-propagating major rainband. The cyclonic systems associated with the BSISO introduces a southwest wind anomaly behind the major rainband, enhancing the orographic rainfall over the WG, and resulting in the phase lag. This lag is not observed in the AY region where more closed cyclonic circulations occur. Diurnal variations in rainfall over the WG regions are smallest during the strongest BSISO rainfall anomaly phase.

1. Introduction

Rainfall during the Asian summer monsoon is concentrated along the western coastal regions of India [Western Ghats (WG)] and Myanmar [Arakan Yoma (AY)] (e.g., Xie et al. 2006; Hoyos and Webster 2007; Romatschke and Houze 2011; Kumar et al. 2014). Rainfall maxima were previously observed offshore in satellite observations (Krishnamurti et al. 1983; Grossman and Garcia 1990). Motivated by these observations, several numerical studies (Smith and Lin 1983; Grossman and Durran 1984; Ogura and Yoshizaki 1988) investigated the rainfall maxima upstream of the WG. More recently, Hoyos and Webster (2007) showed localized rainfall maxima to the west of the WG using data from the Global Precipitation Climatology Project (GPCP) (see their Fig. 2a). With respect to the rainfall near AY, Xie et al. (2006) showed that the rainfall maxima are located approximately 50 km offshore of Myanmar's west coast (see their Fig. 4),[1] using the Tropical Rainfall Measuring Mission (TRMM) Precipitation Radar (PR) data.

While there have been efforts to explain near-coastal rainfall maxima through numerical modeling of the flow interacting with coastal topography, Johnson (2011) suggested a full explanation requires consideration of the diurnal cycle. Over the Indonesian Maritime Continent (IMC), the diurnal cycle is dominant and diurnal-driven offshore migrating systems contribute to rainfall maxima offshore (Mori et al. 2004; Wu et al. 2009; Ichikawa and Yasunari 2006). Motivated by these observations of the diurnal cycle of rainfall concentrations near tropical coastlines, Ogino et al. (2016) modeled the annual mean precipitation in the tropics as a function of coastal distance and noted, ''the principal and fundamental cause of producing the coastal precipitation must be the diurnal land–sea circulation driven by the heat contrast between them'' (p. 1235). Romatschke and Houze (2011), however, showed a weak diurnal cycle over the WG and AY.

Corresponding author: Shoichi Shige, shige@kugi.kyoto-u.ac.jp

[1] This result was due to human errors (S.-P. Xie 2015, personal communication), as shown later.

DOI: 10.1175/JCLI-D-16-0858.1

The boreal summer monsoon intraseasonal oscillation (BSISO) is the dominant large-scale feature of the monsoon (see review in Webster et al. 1998), which in general develops over the equatorial Indian Ocean and propagates northward (Yasunari 1979). Hoyos and Webster (2007) showed that rainfall in AY is produced not only by the in situ and orographic-driven convection, but also by northward-propagating convection within BSISOs. Transient enhanced cyclonic circulations in the northern region of the Bay of Bengal (referred to as Bay of Bengal depressions) associated with BSISOs tend to drive moist air toward the mountain ranges, resulting in rainfall. Hoyos and Webster (2007) suggested that a similar interaction between the BSISO and orography occurs over the WG region, but they did not examine this hypothesis in detail.

For over 16 yr, the TRMM PR, the first spaceborne radar, provided the most reliable precipitation products in the tropics and subtropics through the well-developed 2A25 retrieval algorithm (Iguchi et al. 2009) (see review by Houze et al. 2015). The sampling properties of TRMM PR were poor due to the narrow swath of 215 (245) km before (after) the orbit boost in August 2001, but the 16-yr data accumulation allows us to create a high-resolution rainfall climatology. In this paper, the role of orography, diurnal cycle, and BSISO in determining the characteristics of summer monsoon rainfall over the WG and AY is studied, using the high-resolution rainfall climatology from the TRMM PR observations. Section 2 describes the datasets and methods used in this study. Section 3 revisits the positions of rainfall maxima in the WG and AY regions, and section 4 examines the diurnal cycle in the WG and AY regions as a function of environmental wind conditions. Section 5 describes the interaction between the BSISO and orography, with the focus on the WG region. Section 6 offers a summary of the findings of this paper.

2. Data and methods

In this study, data from the TRMM PR 2A25 version 7 (V7) (Iguchi et al. 2009) for a 16-yr period (1998–2013) during the monsoon months (June–August) on a 0.05° grid are used. To compare the findings presented here with the results of Xie et al. (2006, their Fig. 1b), the 7-yr (1998–2004) averaged June–August climatologies of the surface precipitation from version 6 (V6) of the TRMM PR 3A25, 0.5°-spatial-resolution gridded monthly composite of instantaneous and footprint-scale data (PR 2A25), are also briefly considered. The European Centre for Medium-Range Weather Forecasts (ECMWF) interim reanalysis (ERA-Interim; Dee et al. 2011) dataset was used to describe the atmospheric environment, having a resolution of 0.75° × 0.75° at 6-hourly intervals.

To compare the rainfall maxima determined by the infrared (IR) techniques used by the earlier satellite observations, the Geostationary Operational Environmental Satellite (GOES) Precipitation Index (GPI; Arkin and Meisner 1987) is applied to a single global (60°N–60°S) IR product (Janowiak et al. 2001) for a 14-yr period (2000–13) during the monsoon months (June–August). The GPI assigns a constant conditional rain rate of 3 mm h^{-1} to all pixels within a given region that have a brightness temperature lower than 235 K and assigns a zero rain rate to all other pixels. The TRMM 3B42 V7 data from TRMM Multisatellite Precipitation Analysis (TMPA; Huffman et al. 2007), the merged microwave–IR product where the rain gauge analysis is indirectly used for the calibration over land, are also used. In TMPA, the GPI method has been used for IR estimates.

To examine the amplitude of the diurnal cycle of rainfall, the normalized relative amplitude (NRA) of the diurnal cycle for the 16-yr period (1998–2013) is derived from the TRMM PR data. This is defined by average evening (1200–2359 LT) minus morning (0000–1159 LT) rainfall, normalized by the climatological mean rainfall, following Johnson (2011) and Rauniyar and Walsh (2011).

The bimodal intraseasonal oscillation index developed by Kikuchi et al. (2012) accurately represents the state of the BSISO and Madden–Julian oscillation (MJO) modes at any particular time of year. The index is based on the extended empirical orthogonal function analysis of 25–90-day filtered daily outgoing longwave radiation data with 2.5° horizontal resolution (Liebmann and Smith 1996). For this study, the eight phases of the BSISO mode defined by Kikuchi et al. (2012) are used. Days on which the amplitude of the BSISO index was larger than 1 are analyzed, resulting in 65% of all days during the monsoon months of the 16-yr period.

Previous studies pointed out that two types of intraseasonal oscillations (10–20 and 30–60 days) are important in the Asian monsoon region (e.g., Annamalai and Slingo 2001), but the 10–20-day mode is beyond the scope of this study. We focus on the interaction between the BSISO and orography over the WG region where Hartmann and Michelsen (1989) showed that only the 30–60-day mode is important, using a 70-yr record of daily rainfall.

3. Position of rainfall maxima

Figures 1a,b show the 16-yr averaged June–August climatologies of the surface precipitation at 0.05° resolution estimated from the PR data and 850-hPa wind velocity from the ERA-Interim data. Rainfall on the

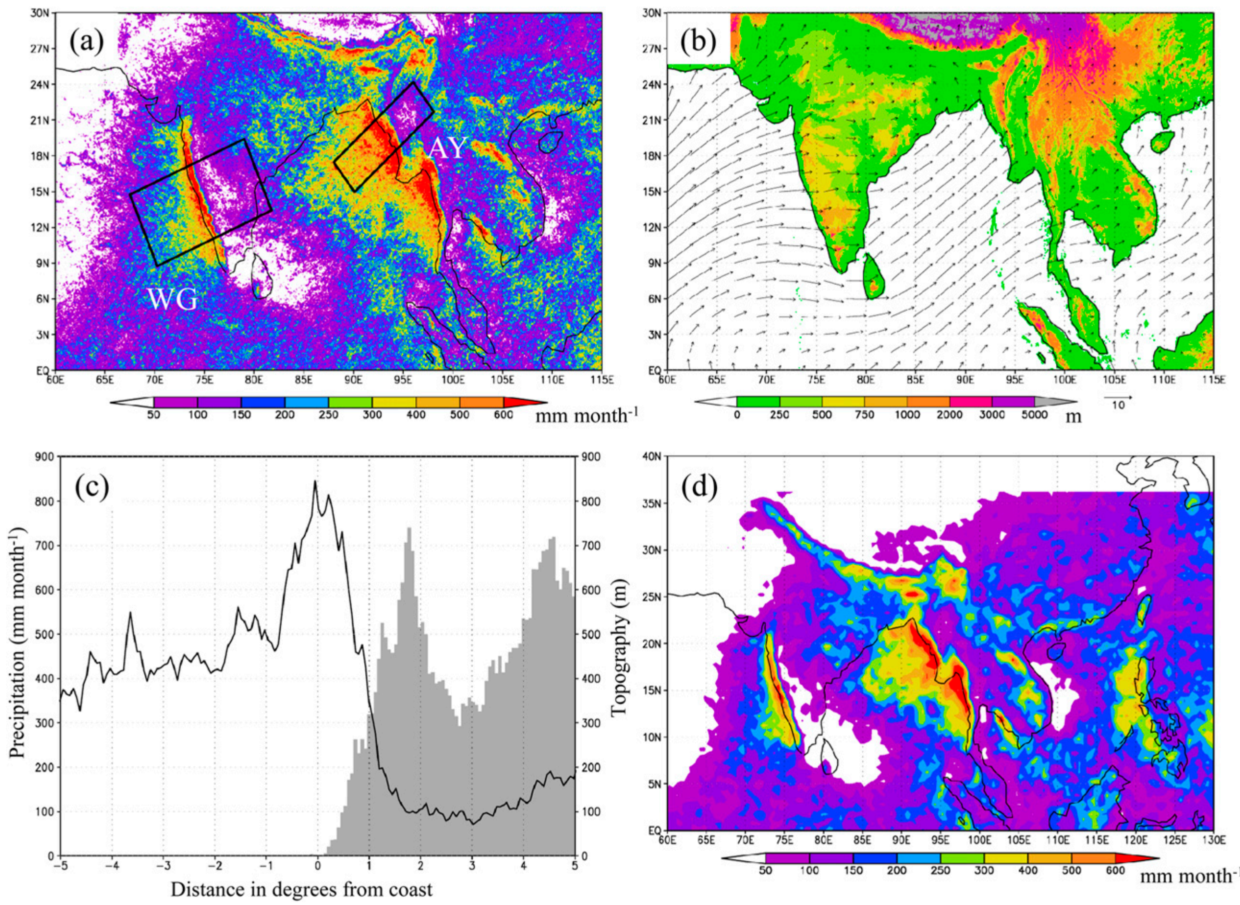

FIG. 1. June–August climatologies of (a) surface precipitation (mm month^{-1}) at 0.05° resolution using the TRMM PR 2A25 V7 data and (b) 850-hPa wind vectors (m s^{-1}) from ERA-Interim with orography (m) for a 16-yr period (1998–2013). The coastal regions of western India [Western Ghats (WG)] and Myanmar [Arakan Yoma (AY)] are indicated by the black boxes in (a). (c) Cross-shore distributions of precipitation (black line; mm month^{-1}) and topography (gray bars; m) averaged across the AY region. (d) The 7-yr (1998–2004) averaged June–August climatologies of surface precipitation at 0.5° resolution from the TRMM PR 2A25 V6 data.

western side of the coastal mountain ranges of western India (WG) and Myanmar (AY), where southwesterly flow impinges during the summer monsoon, are the regions experiencing the highest levels of rainfall. Overall, the patterns of accumulated rain agree with those in Xie et al. (2006, their Fig. 1b) reasonably well. Figure 1a, however, shows that rainfall is highest along the mountain slopes over the WG region while Xie et al. (2006) observed the rainfall maxima offshore of the WG region. Position of rainfall maxima over the AY region is not clear. The cross-shore distribution of rainfall and orography over the AY region is shown in Fig. 1c, which corresponds to Fig. 4 of Xie et al. (2006). In Xie et al. (2006), the maximum rainfall was shown to be displaced windward of the maximum orography by as much as 50 km, but the rainfall maxima are also observed on the coastline in Fig. 1c of the present study. Biasutti et al. (2012) also showed that the maxima in rainfall frequency are not displaced from the upslope of AY and the most frequent precipitation is seen on the coast (see their Fig. 10).

Xie et al. (2006) showed the 7-yr (1998–2004) averaged June–August climatologies of surface precipitation at 0.5° resolution, for the PR data. Though not explicitly noted, the data used by Xie et al. (2006) are likely from V6 of 3A25, for which data processing started in June 2004. The 7-yr (1998–2004) averaged June–August climatologies of surface precipitation at 0.5° resolution from V6 are shown in Fig. 1d. In this figure, we made the format (i.e., domain, color bar, etc.) as consistent as possible with Fig. 1b of Xie et al. (2006), which showed the offshore displacement of rainfall maxima west of the WG and many other locations. The most serious problem in V6 of the PR algorithm was the underestimation of rain over land, in particular, over Africa (Iguchi et al. 2009). Therefore, rainfall over the slopes of the WG from V6 is smaller than that from V7, but the rainfall maxima are still observed over the slopes of the WG.

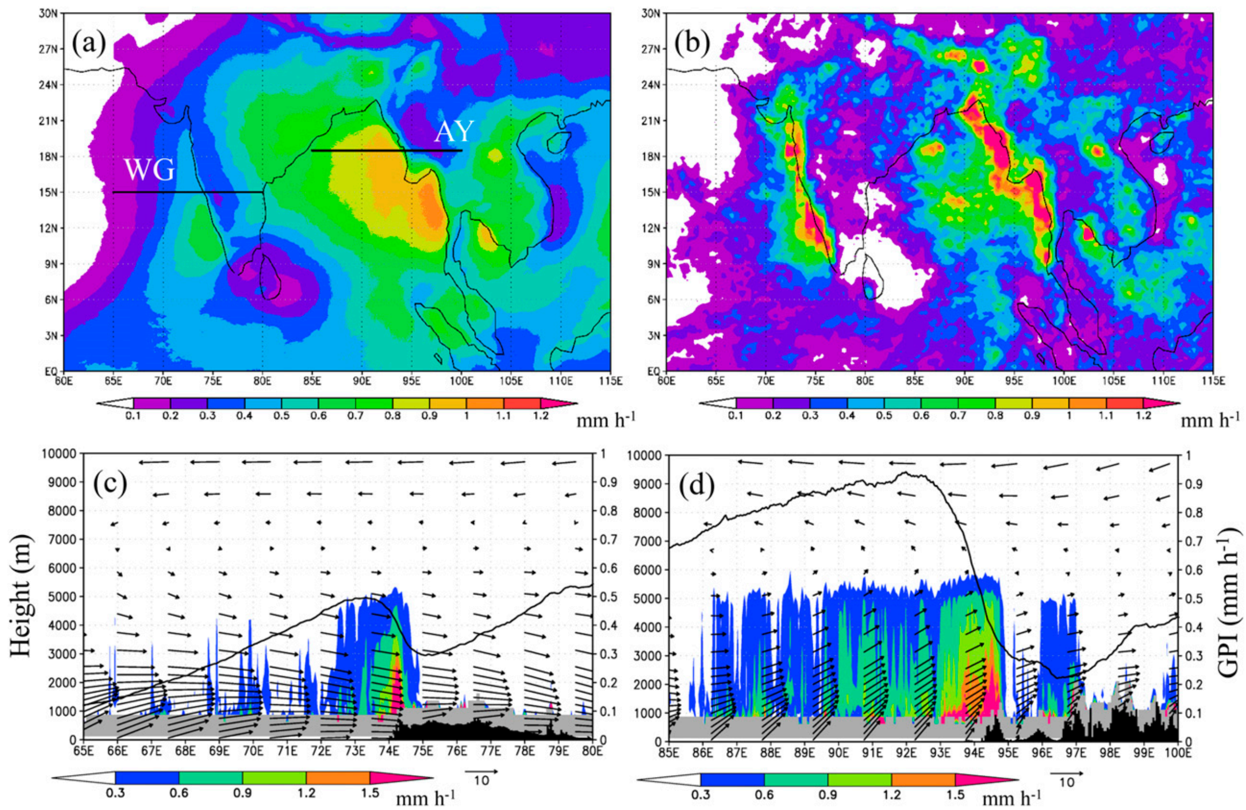

FIG. 2. June–August climatologies of surface precipitation (mm h^{-1}) based on (a) the GPI method for a 14-yr period (2000–13) and (b) TRMM 3B42 data for a 16-yr period (1998–2013). Longitude–height cross sections of the 16-yr June–August unconditional mean precipitation rate (mm h^{-1}) from the TMM PR data and horizontal wind along with topography across the (c) WG and (d) AY regions, which the black lines indicate in (a). Black solid lines in (c) and (d) indicate surface precipitation (mm h^{-1}) based on the GPI method.

Some recent studies have shown reasonable rainfall maximum locations in the WG and AY regions, but they did not discuss them explicitly. For example, Romatschke and Houze (2011, p. 24) showed rainfall maximum locations correctly, but noted, ''The coastal regions of western India and western Myanmar are the regions of greatest monsoon precipitation, with much of the rain falling over the ocean upwind of the coastlines (Hoyos and Webster 2007; Xie et al. 2006).'' This idea might come from the influence of earlier numerical studies (Smith and Lin 1983; Grossman and Durran 1984; Ogura and Yoshizaki 1988), which investigated offshore maxima in rainfall near the WG. The spatial shift of the rainfall away from the WG was determined from images of high reflective clouds by the method of Kilonsky and Ramage (1976; see Fig. 2a of Grossman and Durran 1984) or rain maps produced from infrared radiometers (IR) and gauges by Krishnamurti et al. (1983; see Fig. 1 of Ogura and Yoshizaki 1988).

Figure 2a shows the June–August climatology of surface precipitation from the GPI (Arkin and Meisner 1987), which is a popular IR technique and has been used in the TRMM 3B42 data (Fig. 2b) from TMPA (Huffman et al. 2007). Rainfall maxima offshore with very weak rainfall over the upslope are found in the WG and AY regions, as in the previous studies. To validate the GPI rain maxima, the longitude–height cross sections of the unconditional mean precipitation rate from the PR over the WG and AY regions with ERA-Interim horizontal winds are shown in Figs. 2c,d. The GPI method determined the spatial shift of the rain maxima away from the PR rainfall maxima over both regions. Infrared techniques, such as the GPI method, as well as visible sensor techniques assume that deeper, colder clouds are more likely to produce heavy rainfall, leading to an overestimate of rain area from the cold brightness temperatures associated with extensive cirrus anvils (Ebert and Manton 1998) and an underestimate of the orographic rainfall associated with relatively low and warm cloud tops (Arkin et al. 1989). Rickenbach (1999) showed that in an environment of deep tropospheric directional wind shear, the cold cloud shield became spatially decoupled from the source convection of tropical oceanic squall lines, leading to the poor performance of IR techniques. Strong vertical wind shear with low-level westerlies and upper-level easterlies is

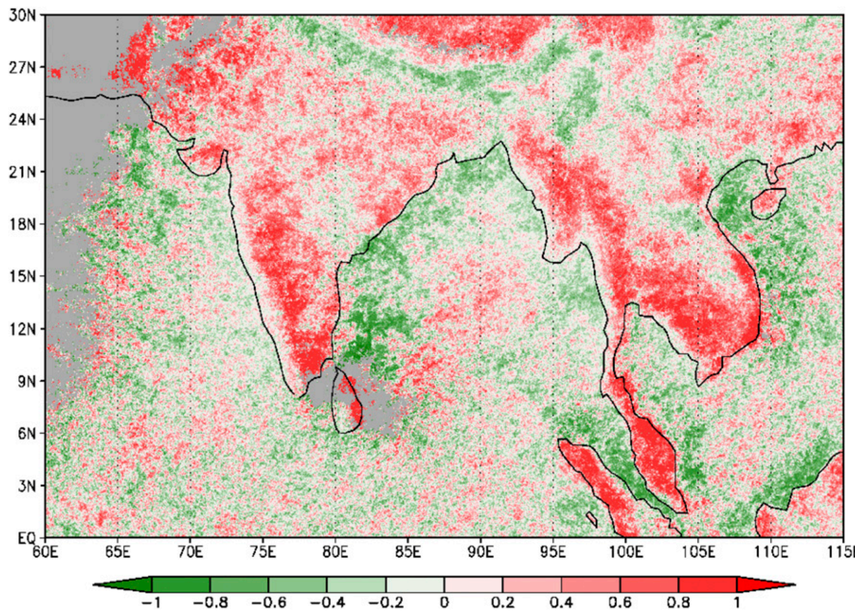

FIG. 3. NRA of the diurnal cycle of rainfall defined by average June–August evening (1200–2359 LT) minus morning (0000–1159 LT) rainfall normalized by June–August mean rainfall for a 16-yr period (1998–2013) using the TRMM PR data. Gray areas indicate the occurrence of raining pixels of <1%.

found in Figs. 2c,d. Thus, the spatial shift of the GPI rain maxima away from the PR rainfall maxima is attributed to westward advection of cirrus anvils from the convection associated with relatively low and warm cloud tops over the upslope by upper-level easterlies.

The rainfall patterns from the TRMM 3B42 data (Fig. 2b) agree much more with the TRMM PR data (Fig. 1a) than those estimated by the GPI method, but the rainfall maxima occur offshore of the WG region instead of the upslope. Over coastal mountain ranges of the Asian monsoon region, heavy orographic rainfall associated with low precipitation-top heights (Shige and Kummerow 2016; Konwar et al. 2014) leads to conspicuous underestimation of rainfall using microwave radiometer algorithms, which conventionally assume that heavy rainfall is associated with high precipitation-top heights (Shige et al. 2013, 2015; Taniguchi et al. 2013; Yamamoto and Shige 2015; Yamamoto et al. 2017). Over land, the rain gauge analysis is indirectly used to create the TRMM 3B42 data, but there still remained underestimation over the upslope of the WG region by the microwave radiometer algorithm (Kummerow et al. 2015) used in the TMPA (see Figs. 2.2d,f of Shige et al. 2015). The GPI method used in the TMPA also contributes to the rainfall maxima offshore of the WG region. The GPI method has been also used in the GPCP data (Adler et al. 2003; Huffman et al. 2001), resulting in the localized rainfall maxima to the west of the WG shown by Hoyos and Webster (2007) (see their Fig. 2a). These data need to be used with care in the Asian summer monsoon region with strong vertical wind shear and the orographic rainfall associated with low cloud tops.

4. Diurnal cycle

The prevailing view that the coastal precipitation in the tropics results from daytime heating over land, which results in land–ocean temperature gradients due to the smaller heat capacity of land compared to that of ocean, is generally attributed to observational studies of the IMC (Ogino et al. 2016; Yamanaka 2016). Diurnal-driven offshore migrating systems contribute to rainfall maxima offshore of the IMC (Mori et al. 2004). In contrast, we have shown the rainfall maxima occur over the upslope of the WG and the coastline of the AY regions instead of offshore, in section 3. In this section, we examine the diurnal cycle of rainfall over the WG and AY regions.

The NRA for June–August over the Asian monsoon region (Fig. 3) shows the general preference for afternoon–evening rainfall over land and morning rainfall over the ocean. Late night–morning rainfall over the southern slopes of the Himalayas is distinct, which is consistent with Hirose and Nakamura (2005). A strong diurnal cycle is found in the IMC, which is consistent with previous studies. In contrast, the upslope of the WG and AY, the regions experiencing the heaviest rainfall during the Asian summer monsoon (Fig. 1a), have very

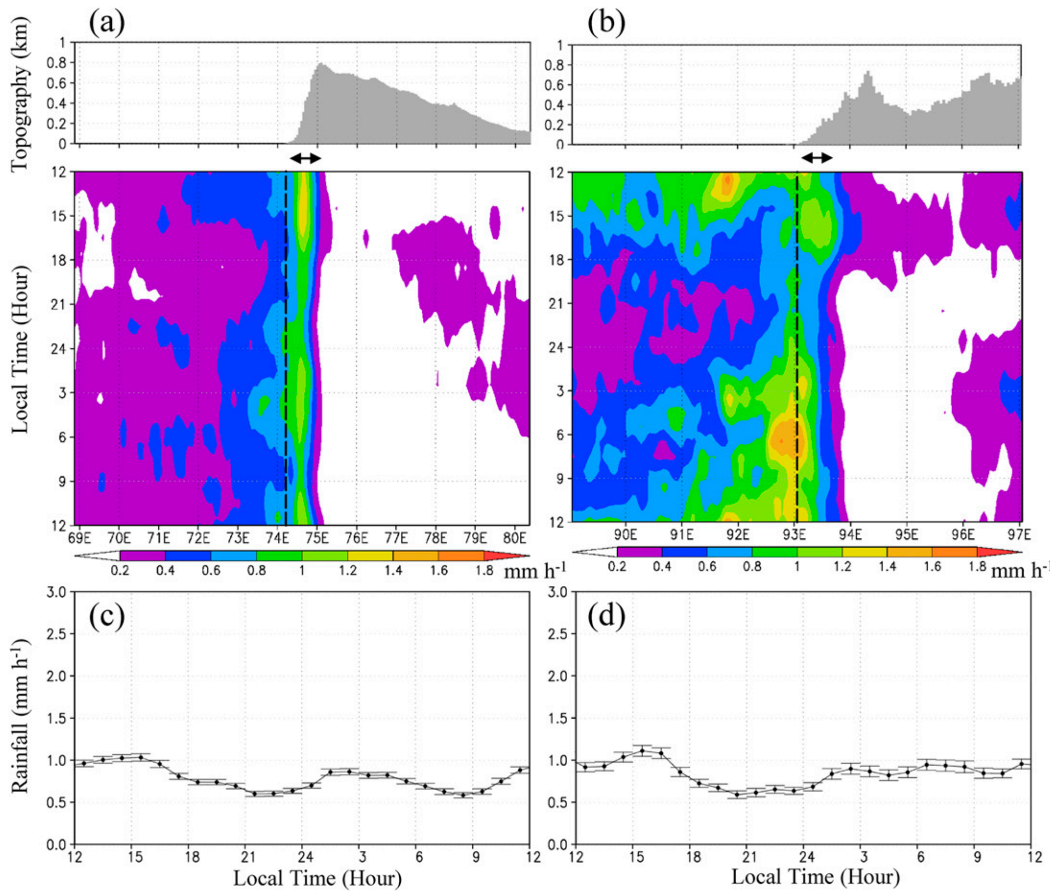

FIG. 4. Time–zonal sections of the composite diurnal rainfall cycle averaged across the (a) WG and (b) AY regions, which are indicated by the black boxes in Fig. 1a, where a 1–2–1 temporal filter is applied. Topography (km) is indicated by the gray bars above the plots. Vertical dashed lines indicate the location of the coast. The mean diurnal variation of rainfall with intervals of error bars indicating the 95% confidence interval for the mean values with the Student's *t* test for the upslope of the (c) WG and (d) AY regions, which are indicated by the arrows in (a) and (b).

small amplitudes, which is consistent with Romatschke and Houze (2011). It should be noted that Johnson (2011) showed evening rainfall for May–June along coastlines over the WG and AY regions using TRMM 3B42 data, cautioning using the data in the Asian summer monsoon region. On the other hand, the leeward sides of the WG and AY have large amplitudes. Weak diurnal cycles over the windward sides and strong cycles over the leeward sides are evident for other coastal mesoscale mountains in the Indochina Peninsula such as Bilauktaung, Cardamom, and the Annam Range.

Regional variations in the diurnal rainfall cycle observed by the PR averaged over the domains perpendicular to the WG and AY (Fig. 1a) are shown in Fig. 4. The narrow rainfall area over the upslope of the WG (Fig. 4a) indicates pure orographic rainfall over the WG. Continuous rain with a slight nocturnal and afternoon–evening maxima is found over the upslope of the WG (Fig. 4a), resulting in a double-peaked cycle with small amplitudes over the upslope (Fig. 4c). On the other hand, an afternoon peak over the upslope and a morning peak just off the coast are found in AY (Fig. 4b), resulting in an afternoon peak over the upslope (Fig. 4d). Romatschke and Houze (2011) showed a double-peaked cycle for strong precipitating medium-sized systems occurring in the WG and AY regions (see their Figs. 13b,d), although their selected regions are wider than those used in this study. They speculated that the peak in the afternoon is likely related to systems over land, while the morning peak is likely associated with the behavior of systems over the ocean. This could account for the afternoon peak over the upslope and a morning peak just off the coast in the AY region, but this possibility seems unlikely for the WG region because both peaks are found over the upslope.

As shown in Fig. 3, the diurnal cycles over the WG and AY regions are much weaker than over the IMC. Nugent et al. (2014) showed ambient upstream wind

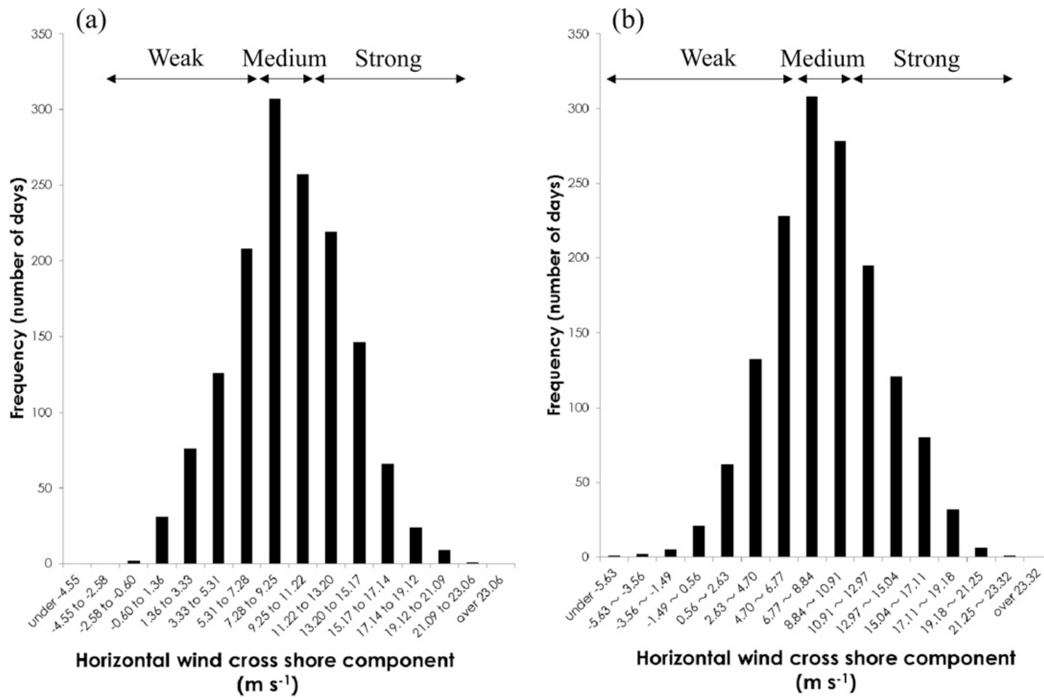

FIG. 5. Histogram showing the frequency (number of days) of the cross-shore component of the horizontal wind (m s^{-1}) averaged over the upstream regions of (a) the WG and (b) AY. The upstream regions are indicated by the black boxes in Fig. 6.

speed control in the transition of tropical orographic convection over Dominica, a small mountainous island in the eastern Caribbean Sea, from low-wind thermal to high-wind mechanical convection. During the summer monsoon, southwesterly flows over the WG and AY regions are much stronger than over the IMC (Fig. 1b). To investigate the wind speed control of convection type (i.e., diurnal cycle amplitude) over coastal mountain ranges, we categorized the TRMM PR data according to ambient upstream wind speed.

Figure 5 shows the frequency of the cross-shore component of upstream horizontal wind (m s^{-1}) at 850 hPa for the WG and AY regions. Three regimes are defined as follows: weak ($U \leq \overline{U} - \sigma$), medium ($\overline{U} - \sigma < U < \overline{U} + \sigma$), and strong ($U \geq \overline{U} + \sigma$) regimes, where U is the cross-shore component of upstream horizontal wind, $\overline{U}$ is the mean of U, and σ is the standard deviation of U. The mean wind speed over the WG (9.25 m s^{-1}) is larger than that for AY (8.84 m s^{-1}), while the standard deviation for the WG (3.94 m s^{-1}) is smaller than that for AY (4.20 m s^{-1}).

The NRA over the coastal areas of the WG and AY regions for the weak wind regime is much larger than that for the strong wind regime (Fig. 6), indicating that the diurnal cycle is a function of ambient upstream wind. The results are consistent with the fact that the thermally forced circulation is typically observed under no or weak environmental wind, while the mechanically forced circulation dominates under strong environmental wind. Banta (1990) suggested that stronger winds ventilate the surface as it tries to heat up, and they produce mechanical turbulence that also mixes the heat away from the surface, preventing the buildup of a strong temperature difference that would drive thermally forced circulations.

Regional variations in the diurnal rainfall cycle averaged over domains perpendicular to the WG and AY (Fig. 1a) for weak and strong regimes are shown in Fig. 7 and Fig. 8, respectively. Rainfall for the weak wind regime over the WG and AY regions is much smaller than that for the strong wind regime, indicating that the contribution of thermally driven convection to rainfall is much smaller than that of mechanically driven convection. For the weak wind regime, rain maxima over the upslope in the afternoon and rain maxima over the ocean at midnight and in the early morning are seen for the WG and AY regions (Figs. 7a,b), leading to a one-peaked cycle over the upslope (Figs. 7c,d). The continuous rain with slight nocturnal and afternoon–evening maxima for the strong wind regime over the upslope of the WG (Figs. 8a,c) is very similar to that for all regimes over the WG shown in Figs. 4a,c except for larger rainfall amounts. Again, mechanically driven convection is a major contributor to rainfall, and therefore rainfall is concentrated over the upslope of the WG regions. Over

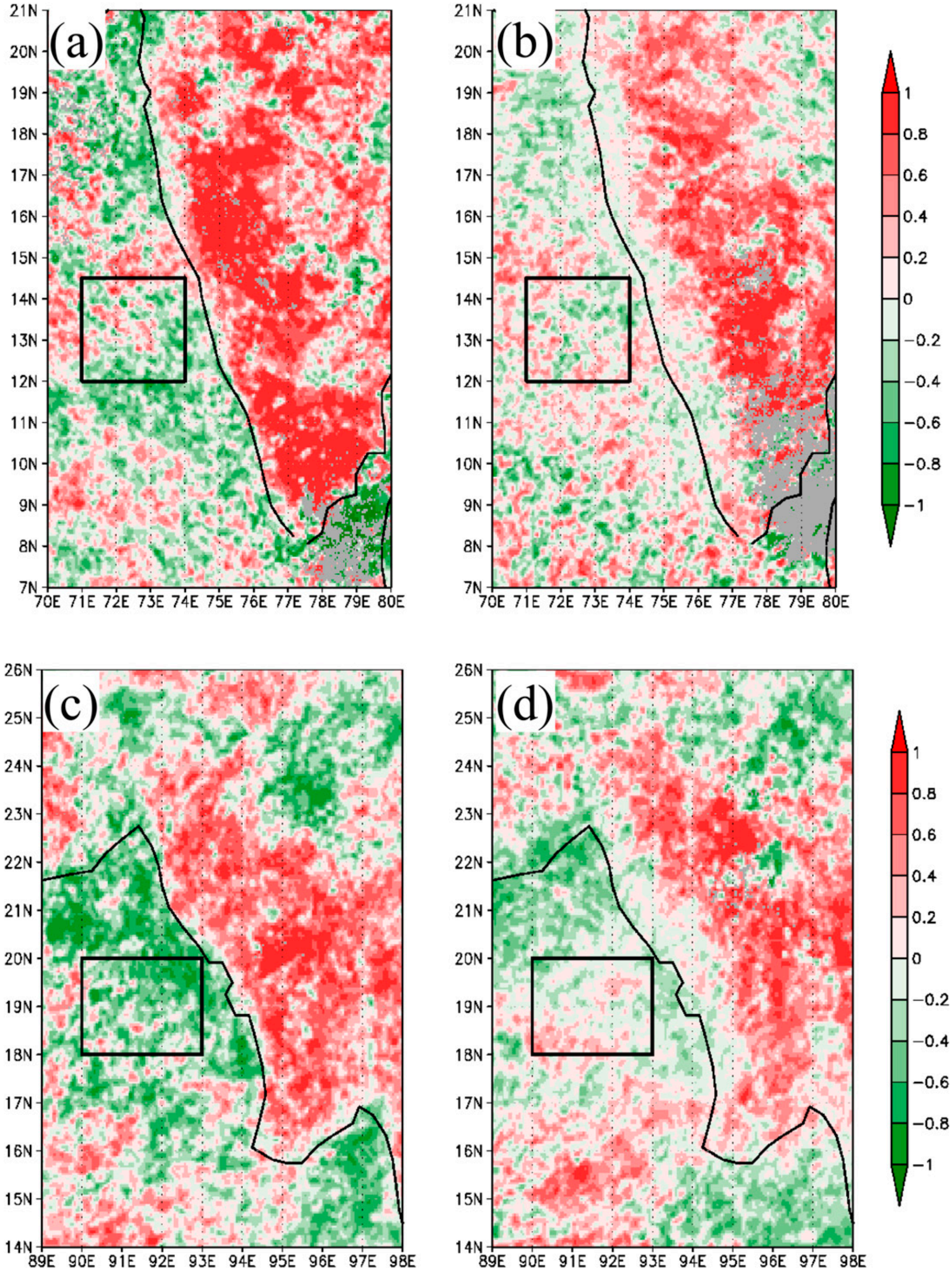

FIG. 6. NRA of the diurnal cycle of rainfall during June–August for the (left) weak and (right) strong cross-shore component of the horizontal wind regime for (a),(b) the WG and (c),(d) the AY. The upstream regions for cross-shore components of the horizontal wind are indicated by the black boxes. Gray areas indicate the occurrence of raining pixels <1%.

AY, morning and slight afternoon maxima over the coast are seen for the strong wind regime (Figs. 8b,d).

According to the classical view of orographically and thermally forced winds in mountains (Lin 2007), during the day, the mountain serves as an elevated heat source because of the sensible heat released by mountain surface. In a quiescent atmosphere, this can induce mountain upslope flow, leading to the rain maximum over the

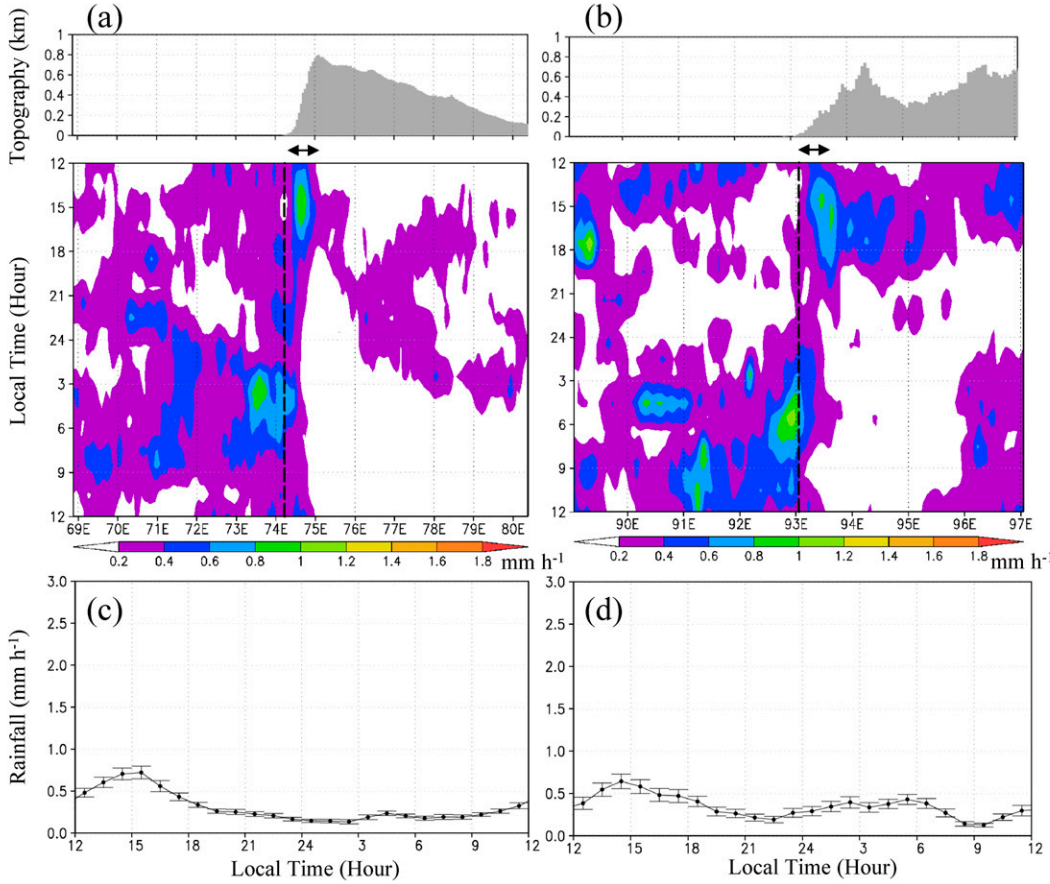

FIG. 7. As in Fig. 4, but for the weak wind regime.

upslope in the afternoon. At night, the opposite occurs: surface cooling produces downslope flow. Diurnal components of surface wind (surface divergence) are calculated as the difference between the 6-houly surface wind (surface divergence) and the daily mean surface wind (surface divergence) for the weak and strong wind regimes for the WG and AY regions, using the data from ERA-Interim for a 16-yr period (1998–2013). At 0000 UTC (0500 LT for the WG and 0600 LT for the AY), the diurnal components of the surface winds over the coastal mountains of the WG and AY regions flow toward the oceans for weak and strong wind regimes (Fig. 9). It is likely that the diurnal components of the surface winds in the early morning are downslope flows. The downslope flows over the WG and AY regions for the weak wind regime are stronger than those for the strong wind regime, resulting in the shift of convergence over the upslope for the strong regime to that just off the coast for the weak regime. Therefore, the rain maximum just off the coast at midnight and in the early morning for the weak wind regime is attributed to the downslope flow.

Over AY, rainfall with a midday maximum is enhanced over the ocean (91°–92°E) for the strong wind regime (Fig. 8b) compare to all regimes shown in Fig. 4b. Romatschke and Houze (2011) showed that large systems in the Bay of Bengal region formed when cyclonic circulations (Bay of Bengal depressions) enhanced the anomalous southwesterly flow and have a strong diurnal cycle with a midday maximum. They speculated that the initial convection of the mesoscale system is triggered over the ocean during the late night or early morning, and the nocturnally formed systems off the coast grow until about midday, with expanding stratiform rain areas, as in the case of Borneo (Churchill and Houze 1984; Houze et al. 1981; Williams and Houze 1987) where widespread rainfall is likely related to the presence of the Borneo vortex (Ichikawa and Yasunari 2006). The results for the strong wind regime suggest in situ orographically driven convection (pure orographic rainfall) over the WG region and orographic enhancement of preexisting systems over the AY region, reflecting differences in the latent heating profiles (Fig. 3 of Shige and Kummerow 2016) between the WG (bottom heavy) and AY (top heavy) and resulting in different locations of the rainfall maxima for the WG (upslope) and AY (coastline).

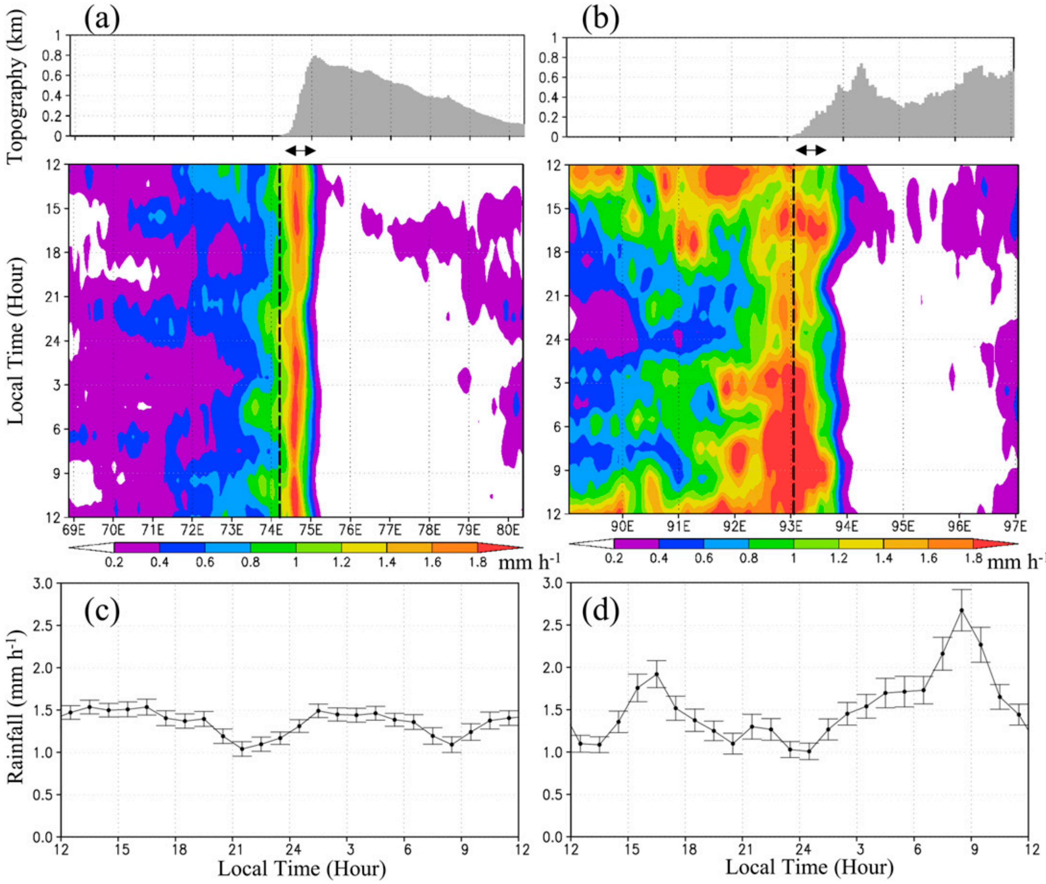

FIG. 8. As in Fig. 4, but for the strong wind regime.

5. BSISO

Figure 10 presents the composite eight-phase BSISO life cycle of the PR rainfall anomalies and ERA-Interim specific humidity anomalies with 850-hPa wind anomalies. The positive rainfall anomaly associated with cyclonic systems forms over equatorial India in phase 1 and moves northward over the Arabian Sea and the Bay of Bengal. The typical northward-propagating character of the BSISO is consistent with previous studies (e.g., Wang et al. 2006; Chattopadhyay et al. 2009). Figure 10 shows the rain anomaly maximum phase band is oriented from northwest to southeast. The northwest–southeast-tilted structure of the major rainband is also consistent with previous studies. It is interesting to note that the rain anomaly over the WG slope is isolated from the major rainband associated with the BSISO. In phase 3, there are positive specific humidity anomalies and positive rainfall anomalies over the surrounding Arabian Sea (Fig. 10k) but negative rainfall anomalies over the WG slope with easterly anomalies (Fig. 10c). Positive rainfall anomalies with westerly anomalies appear over the coast of the WG region in phase 4 (Fig. 10d) and then spread northward in phase 5 (Fig. 10e). The horizontal wind anomaly is a key factor determining the rainfall anomaly associated with BSISO. This feature is consistent with Hartmann and Michelsen (1989) using the rain gauge data, but was not reported in Wang et al. (2006, see their Fig. 2) and Chattopadhyay et al. (2009, see their Fig. 3), since Wang et al. (2006) used only rainfall over the ocean from TRMM Microwave Imager (TMI) and Chattopadhyay et al. (2009) used TRMM 3G68 with a resolution of 0.5° × 0.5° from the PR with a 1–2–1 spatial filter both in the zonal and meridional orientations.

Figure 11 clearly shows that the upslope rain lags behind the offshore rain associated with the BSISO major rainband in the WG region, in contrast to the maxima in the rainfall anomaly over the IMC ahead of the MJO major rainband (Rauniyar and Walsh 2011). The cyclonic systems (Fig. 11c) associated with the BSISO introduce southwest winds (Fig. 11a) behind the major rainband, enhancing the orographic rainfall over the WG, and resulting in the phase lag of rainfall between the Arabian Sea and the WG. Hartmann and

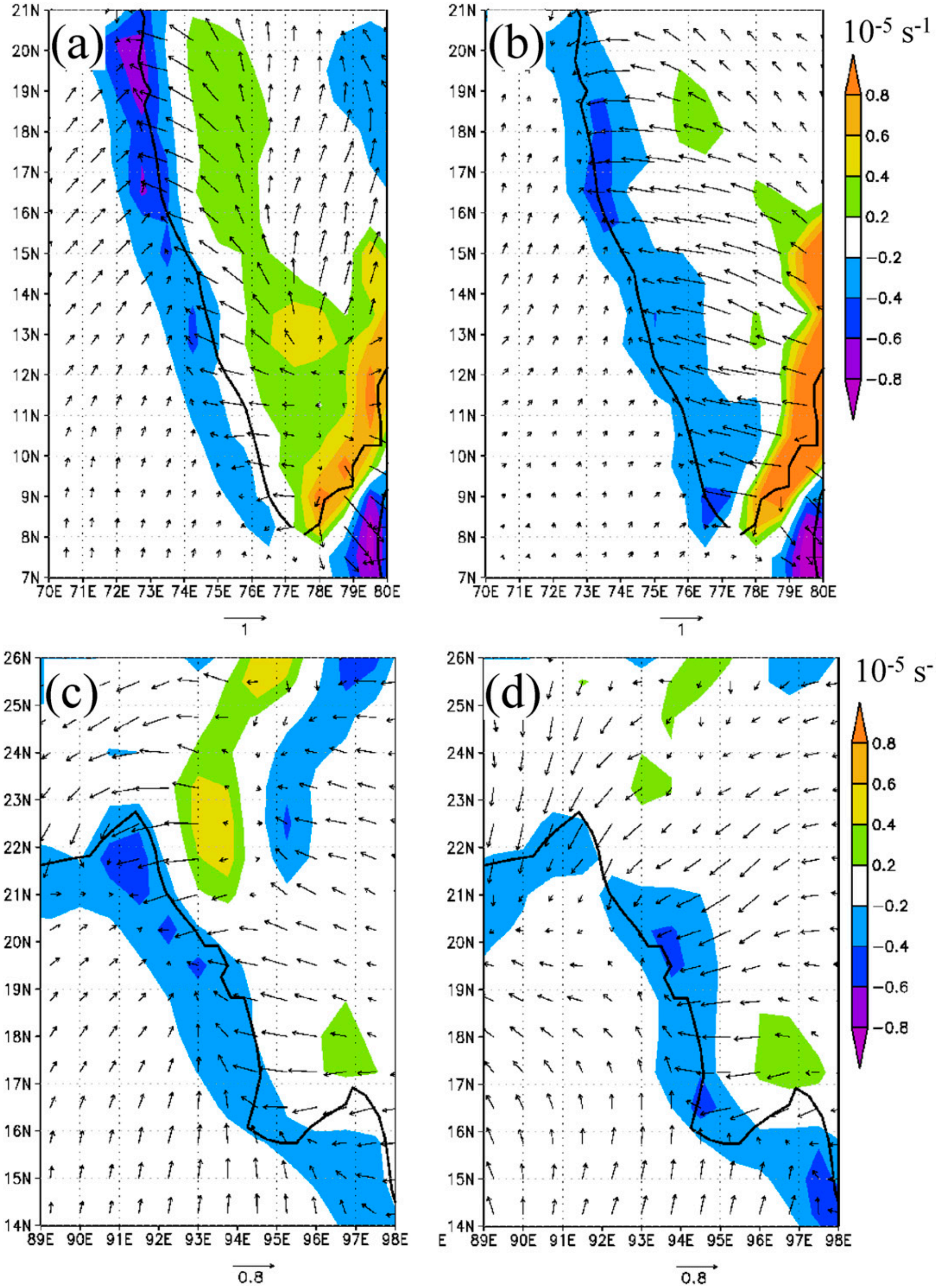

FIG. 9. Diurnal components of surface wind (m s^{-1}) and surface divergence (10^{-5} s^{-1}) at 0000 UTC during June–August for the (left) weak and (right) strong wind regime for (a),(b) the WG and (c),(d) the AY.

Michelsen (1989) showed simultaneous occurrence of the rainfall maximum in the WG region with westerly wind anomaly, although they did not report the phase lag of rainfall between the Arabian Sea and the WG because they used rain gauge data only over the land. This is similar to in-phase relationship between the ground-based radar reflectivity and zonal wind anomalies over the west coast of the Downa range in the western part of the Indochina Peninsula (Yokoi and Satomura 2008). Figure 10g shows that the cyclonic

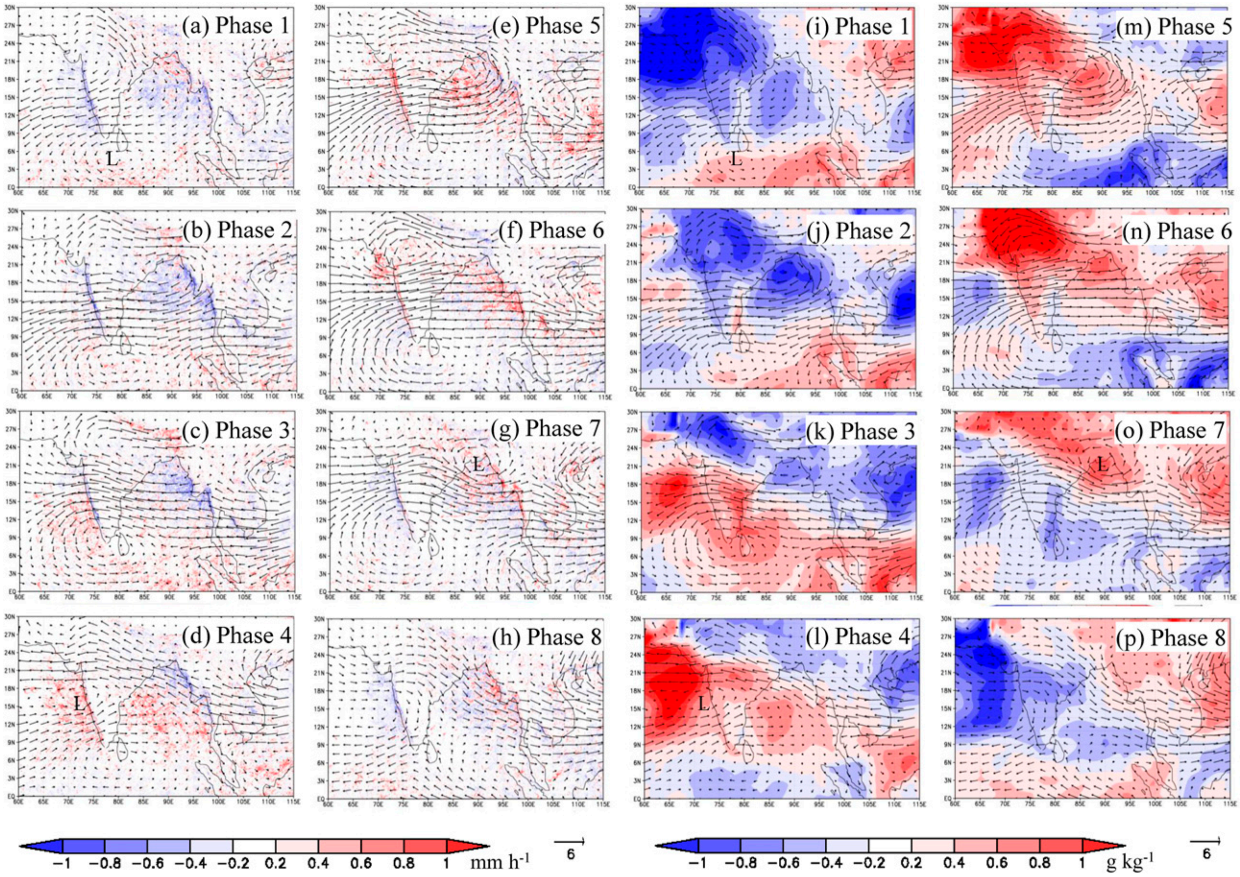

FIG. 10. (a)–(h) PR rainfall anomaly and (i)–(p) ERA-Interim specific humidity anomaly with ERA-Interim 850-hPa wind (m s^{-1}; vectors) during the eight BSISO phases. The L indicates the cyclonic systems referred to in the text.

system over the AY introduces a westerly wind anomaly, enhancing the orographic rainfall over the west coast of the Downa range.

Hoyos and Webster (2007) suggested that the interaction between the BSISO and the orography are similar over the WG and AY regions, but the phase lags among upslope rain, offshore rain, and wind are not observed over the AY region. This is because cyclonic circulations over the AY region during the active phase (Fig. 10g) exhibit smaller expansion and more closed structures than those over the WG region during the active phase (Fig. 10d), leading to much higher relative vorticities over the AY region (Fig. 11d) than over the WG region (Fig. 11c). Large precipitating systems prevail over the Bay of Bengal (Hirose and Nakamura 2005; Romatschke and Houze 2011), resulting in top-heavy heating profiles produced by deep stratiform ice clouds (Fig. 3 of Shige and Kummerow 2016), and enhancing the northward propagation of the BSISO and cyclonic circulations (Chattopadhyay et al. 2009; Choudhury and Krishnan 2011). Differences in precipitating system characteristics and their associated large-scale response might explain the differences in the interaction between the BSISO and orography between the WG and AY regions.

The averaged upstream winds throughout all phases of BSISO shown in Fig. 11a are within the medium wind regime in Fig. 5, but the weak wind regime tends to occur in association with phases 1–2, while the strong wind regime occurs in association with phases 5–6, which affect the diurnal cycle of rainfall as discussed in section 4. Scale interactions on diurnal, intraseasonal, and seasonal time scales is important for the mean and variability of the tropical climate system (see a review by Slingo et al. 2003). A number of studies have investigated the impact of the MJO on the diurnal cycle of rainfall (e.g., Sui and Lau 1992; Tian et al. 2006), but much less attention has been paid to the impact of the BSISO on the diurnal cycle of rainfall. It is interesting to compare the impact of the BSISO on the diurnal cycle of rainfall over the WG with the impact of MJO on the diurnal cycle of rainfall over the IMC.

Again, the phase lag over the WG is clearly visible (Fig. 12a). The modulation of the NRA by the BSISO is evident over the upslope of the WG (Fig. 12b). The

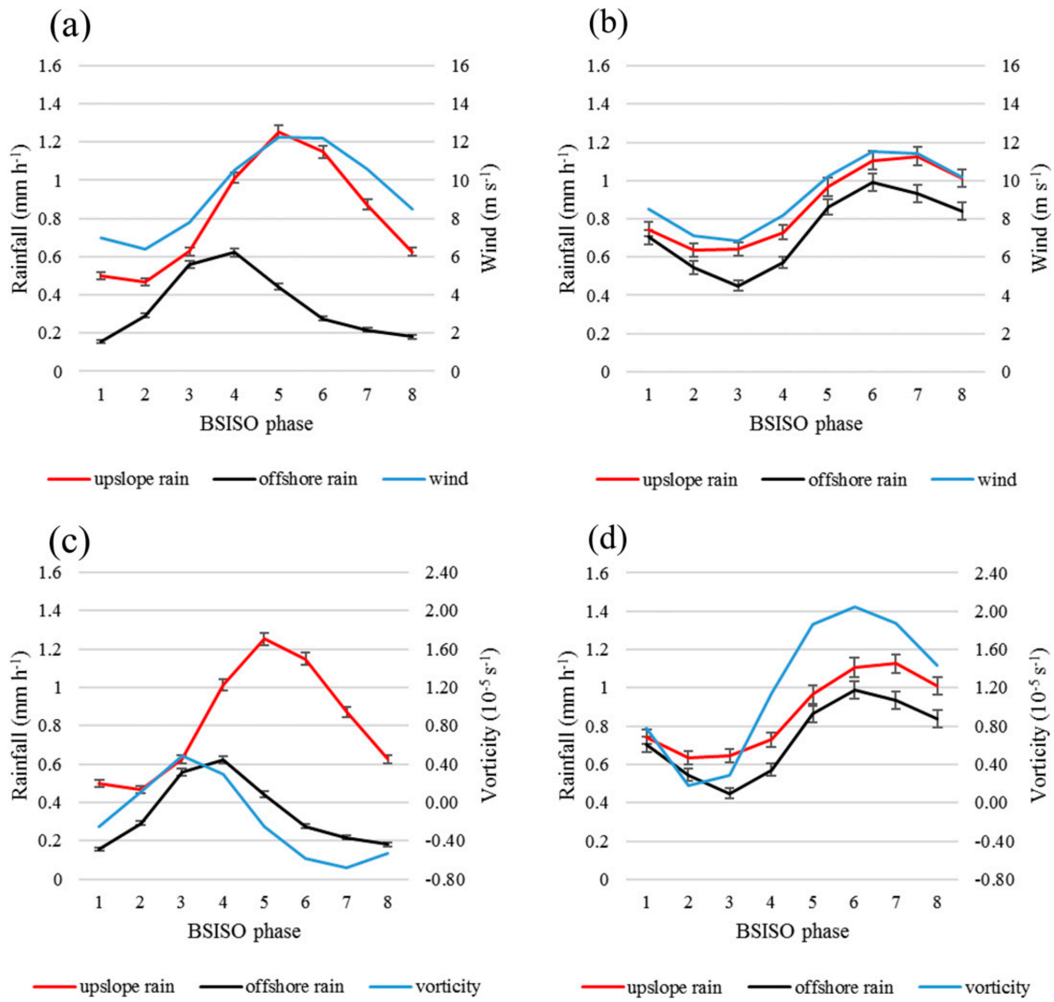

FIG. 11. Upslope rainfall, offshore rainfall, and upstream wind over (a) the WG and (b) AY regions as a function of the composite life cycle of the BSISO. A 1–2–1 temporal filter is applied. (c),(d) As in (a),(b) but with vorticity plotted instead of wind speed. The upslope of the WG and AY regions correspond to that in Fig. 4 and the offshore is located 2° upstream of the upslope, which is indicated in Fig. 12 for the WG.

smallest NRA over the upslope of the WG coincides with the maxima of the BSISO rainfall anomaly during phase 5. Strong winds amplify the mechanically driven convection resulting in the largest BSISO rainfall anomaly over the upslope of the WG, but reduce the thermally driven convection resulting in the smallest NRA over this region. These results are consistent with those in section 4. The NRA over the upslope of the WG is greatest during phase 3, which is before the largest BSISO rainfall anomaly during phase 5, and coincides with the large-scale active BSISO envelope with the largest rainfall anomaly over the surrounding Arabian Sea.

Although there have been disputes on the impact of the diurnal cycle of rainfall by the MJO, Peatman et al. (2014) showed that the amplitude of the diurnal cycle and the daily mean rainfall over the IMC are greatest shortly before the large-scale active MJO envelope arrives, with a lead time of one-eighth of an MJO cycle, in agreement with ground-based observations over the eastern Indian Ocean off the island of Sumatra (Fujita et al. 2011; Kamimera et al. 2012). Therefore, the change in the diurnal cycle of rainfall throughout an intraseasonal cycle is different between the IMC where the diurnal cycle of rainfall is strong and the WG where the diurnal cycle of rainfall is weak and orographic rainfall is strong.

6. Summary

In this study, a TRMM PR dataset of 16 yr is used to explore the physical mechanisms determining the spatial and temporal patterns of summer monsoon rainfall in

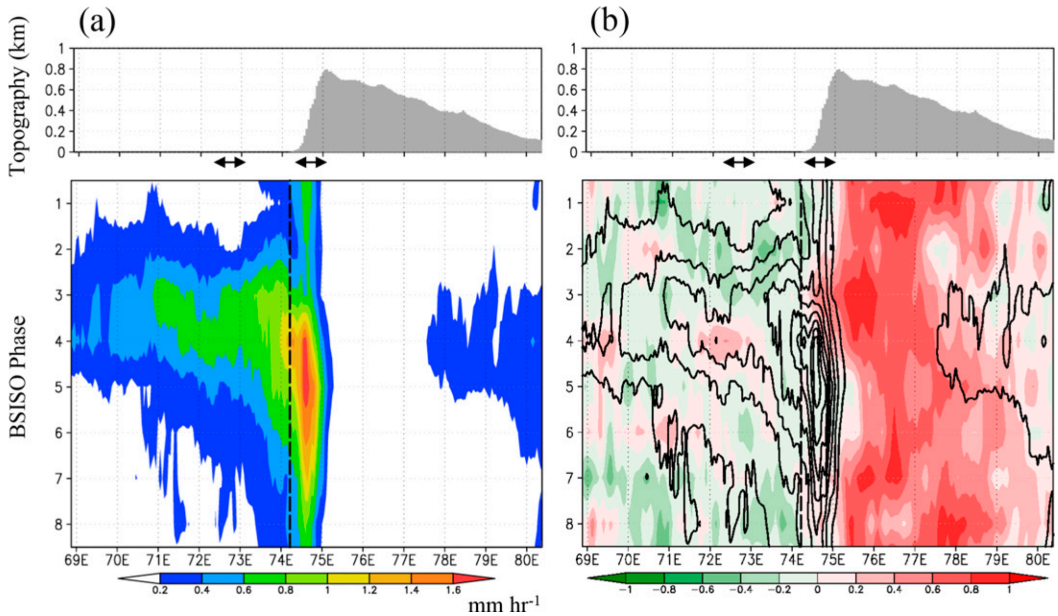

FIG. 12. Time–zonal sections of (a) rainfall and (b) NRA of the diurnal cycle of rainfall associated with the composite life cycle of the BSISO averaged across the WG. A 1–2–1 temporal filter is applied. Topography (m) is indicated by the gray bars above the plots. Vertical dashed lines indicate the location of the coast. Rainfall associated with composite life cycle of the BSISO is shown by black contours in (b). The offshore and upslope are indicated by the arrows.

the WG and AY regions. Satellite observations in previous studies showed that the rainfall maxima occur upstream of the WG and AY (Krishnamurti et al. 1983; Grossman and Garcia 1990; Xie et al. 2006; Hoyos and Webster 2007). In contrast, the TRMM PR data show that the rainfall maxima occur over the upslope of the WG and on the coast of AY. Previous studies using IR data assumed that heavy rainfall results from deep convection, leading to an overestimate of the rain area from the cold brightness temperatures associated with extensive cirrus anvils and an underestimate of the orographic rainfall associated with relatively low cloud tops. The spatial shift of the IR-derived rain maxima away from the PR rainfall maxima is attributed to westward advection of cirrus anvils from the convection associated with relatively low and warm cloud tops over the upslope by upper-level easterlies.

Over the IMC, the diurnal cycle of rainfall is dominant and diurnal-driven migrating systems contribute to the rainfall maxima offshore (Mori et al. 2004; Ogino et al. 2016; Yamanaka 2016). In contrast, diurnal variations in the rainfall are very weak in the WG and AY regions where low-level monsoon flow is strong. Continuous rain with a slight nocturnal and afternoon–evening maxima occurs over the upslope of the WG, while an afternoon peak over the upslope and a morning peak just off the coast are found in AY, resulting in different locations of the rainfall maxima for the WG (upslope) and AY (coastline). The rainfall amount and diurnal cycle amplitude are functions of the environmental flow perpendicular to coastal mountains. Large rainfall amounts but small diurnal amplitudes are observed under strong environmental flow, and vice versa, implying that rainfall is not associated with thermally driven convection, but rather with mechanically driven convection. Ventilation of the surface by stronger winds may prevent the buildup of a strong temperature difference that would drive thermally forced circulations (Banta 1990).

Consistent with past studies, the TRMM PR composites show the northwest–southeast-tilted structure and northward propagation of the major rainband associated with the BSISO. The rain anomaly over the WG lags behind the major rainband, which was not reported by the previous studies (Wang et al. 2006; Chattopadhyay et al. 2009). Orographic rainfall over the WG slope is enhanced with southwesterly wind anomalies of the cyclonic system associated with the BSISO. Hoyos and Webster (2007) suggested that an interaction between the BSISO and orography over the WG is similar to that over AY, but this lag is not observed in the AY region where more closed cyclonic circulations and more stratiform rainfall regions prevail compared to the WG region. The amplitude of the diurnal cycle over the upslope of the WG is smallest during the largest BSISO rainfall anomaly phase over the WG, and it is largest during the large-scale active BSISO phase with the largest rainfall anomaly over the surrounding Arabian Sea, preceding the largest BSISO rainfall anomaly over the WG.

Numerical prediction of the Asian summer monsoon, the world's most energetic monsoon and thus a major component of global climate dynamics, is very important for society. The spatial and temporal nature of summer monsoon rainfall in the WG and AY region described in this paper would be a critical test for climate models.

Acknowledgments. We would like to dedicate this article to the memory of the late Professor Takehiko Satomura, whose research motivated us to start this study. This study is supported by JSPS KAKENHI Grant 26282109 and the JAXA Precipitation Measuring Mission (PMM) Project. Profs. S. Yoden, M. Satoh, Y. N. Takayabu, and M. Hirose are thanked for useful discussions. The authors thank Dr. S. Yokoi, and two anonymous reviewers for their constructive comments that improved the clarity of the paper.

REFERENCES

Adler, R. F., and Coauthors, 2003: The version-2 Global Precipitation Climatology Project (GPCP) Monthly Precipitation Analysis (1979–present). *J. Hydrometeor.*, **4**, 1147–1167, doi:10.1175/1525-7541(2003)004<1147:TVGPCP>2.0.CO;2.

Annamalai, H., and J. M. Slingo, 2001: Active/break cycles: Diagnosis of the intraseasonal variability of the Asian summer monsoon. *Climate Dyn.*, **18**, 85–102, doi:10.1007/s003820100161.

Arkin, P. A., and B. N. Meisner, 1987: The relationship between large-scale convective rainfall and cold cloud over the Western Hemisphere during 1982–84. *Mon. Wea. Rev.*, **115**, 51–74, doi:10.1175/1520-0493(1987)115<0051:TRBLSC>2.0.CO;2.

——, A. K. Rao, and R. R. Kelkar, 1989: Large-scale precipitation and outgoing longwave radiation from INSAT-1B during the 1986 southwest monsoon season. *J. Climate*, **2**, 619–628, doi:10.1175/1520-0442(1989)002<0619:LSPAOL>2.0.CO;2.

Banta, R. M., 1990: The role of mountain flows in making clouds. *Atmospheric Processes over Complex Terrain, Meteor. Monogr.*, No. 45, Amer. Meteor. Soc., 229–283.

Biasutti, M., S. E. Yuter, C. D. Burleyson, and A. H. Sobel, 2012: Very high resolution rainfall patterns measured by TRMM precipitation radar: Seasonal and diurnal cycles. *Climate Dyn.*, **39**, 239–258, doi:10.1007/s00382-011-1146-6.

Chattopadhyay, R., B. N. Goswami, A. K. Sahai, and K. Fraedrich, 2009: Role of stratiform rainfall in modifying the northward propagation of monsoon intraseasonal oscillation. *J. Geophys. Res.*, **114**, D19114, doi:10.1029/2009JD011869.

Choudhury, A. D., and R. Krishnan, 2011: Dynamical response of the South Asian monsoon trough to latent heating from stratiform and convective precipitation. *J. Atmos. Sci.*, **68**, 1347–1363, doi:10.1175/2011JAS3705.1.

Churchill, D. D., and R. A. Houze Jr., 1984: Development and structure of winter monsoon cloud clusters on 10 December 1978. *J. Atmos. Sci.*, **41**, 933–960, doi:10.1175/1520-0469(1984)041<0933:DASOWM>2.0.CO;2.

Dee, D. P., and Coauthors, 2011: The ERA-Interim reanalysis: Configuration and performance of the data assimilation system. *Quart. J. Roy. Meteor. Soc.*, **137**, 553–597, doi:10.1002/qj.828.

Ebert, E. E., and M. J. Manton, 1998: Performance of satellite rainfall estimation algorithms during TOGA COARE. *J. Atmos. Sci.*, **55**, 1537–1557, doi:10.1175/1520-0469(1998)055<1537:POSREA>2.0.CO;2.

Fujita, M., K. Yoneyama, S. Mori, T. Nasuno, and M. Satoh, 2011: Diurnal convection peaks over the eastern Indian Ocean off Sumatra during different MJO phases. *J. Meteor. Soc. Japan*, **89A**, 317–330, doi:10.2151/jmsj.2011-A22.

Grossman, R. L., and D. R. Durran, 1984: Interaction of low-level flow with the Western Ghat Mountains and offshore convection in the summer monsoon. *Mon. Wea. Rev.*, **112**, 652–672, doi:10.1175/1520-0493(1984)112<0652:IOLLFW>2.0.CO;2.

——, and O. Garcia, 1990: The distribution of deep convection over ocean and land during the Asian summer monsoon. *J. Climate*, **3**, 1032–1044, doi:10.1175/1520-0442(1990)003<1032:TDODCO>2.0.CO;2.

Hartmann, D. L., and M. L. Michelsen, 1989: Intraseasonal periodicities in Indian rainfall. *J. Atmos. Sci.*, **46**, 2838–2862, doi:10.1175/1520-0469(1989)046<2838:IPIIR>2.0.CO;2.

Hirose, M., and K. Nakamura, 2005: Spatial and diurnal variation of precipitation systems over Asia observed by the TRMM Precipitation Radar. *J. Geophys. Res.*, **110**, D05106, doi:10.1029/2004JD004815.

Houze, R. A., S. G. Geotis, F. D. Marks, and A. K. West, 1981: Winter monsoon convection in the vicinity of North Borneo. Part I: Structure and time variation of the clouds and precipitation. *Mon. Wea. Rev.*, **109**, 1595–1614, doi:10.1175/1520-0493(1981)109<1595:WMCITV>2.0.CO;2.

——, K. L. Rasmussen, M. D. Zuluaga, and S. R. Brodzik, 2015: The variable nature of convection in the tropics and subtropics: A legacy of 16 years of the Tropical Rainfall Measuring Mission satellite. *Rev. Geophys.*, **53**, 994–1021, doi:10.1002/2015RG000488.

Hoyos, C. D., and P. J. Webster, 2007: The role of intraseasonal variability in the nature of Asian monsoon precipitation. *J. Climate*, **20**, 4402–4424, doi:10.1175/JCLI4252.1.

Huffman, G. J., R. F. Adler, M. M. Morrissey, D. T. Bolvin, S. Curtis, R. Joyce, B. McGavock, and J. Susskind, 2001: Global precipitation at one-degree daily resolution from multisatellite observations. *J. Hydrometeor.*, **2**, 36–50, doi:10.1175/1525-7541(2001)002<0036:GPAODD>2.0.CO;2.

——, and Coauthors, 2007: The TRMM Multisatellite Precipitation Analysis (TMPA): Quasi-global, multiyear, combined-sensor precipitation estimates at fine scales. *J. Hydrometeor.*, **8**, 38–55, doi:10.1175/JHM560.1.

Ichikawa, H., and T. Yasunari, 2006: Time–space characteristics of diurnal rainfall over Borneo and surrounding oceans as observed by TRMM-PR. *J. Climate*, **19**, 1238–1260, doi:10.1175/JCLI3714.1.

Iguchi, T., T. Kozu, J. Kwiatkowski, R. Meneghini, J. Awaka, and K. Okamoto, 2009: Uncertainties in the rain profiling algorithm for the TRMM precipitation radar. *J. Meteor. Soc. Japan*, **87A**, 1–30, doi:10.2151/jmsj.87A.1.

Janowiak, J. E., R. J. Joyce, and Y. Yarosh, 2001: A real-time global half-hourly pixel-resolution infrared dataset and its applications. *Bull. Amer. Meteor. Soc.*, **82**, 205–217, doi:10.1175/1520-0477(2001)082<0205:ARTGHH>2.3.CO;2.

Johnson, R. H., 2011: Diurnal cycle of monsoon convection. *The Global Monsoon System: Research and Forecasts*, 2nd ed. C.-P. Chang et al., Eds., World Scientific Publishing Company, 257–276.

Kamimera, H., S. Mori, M. D. Yamanaka, and F. Syamsudin, 2012: Modulation of diurnal rainfall cycle by the Madden–Julian oscillation based on one-year continuous observations with a meteorological radar in West Sumatera. *SOLA*, **8**, 111–114, doi:10.2151/sola.2012-028.

Kikuchi, K., B. Wang, and Y. Kajikawa, 2012: Bimodal representation of the tropical intraseasonal oscillation. *Climate Dyn.*, **38**, 1989–2000, doi:10.1007/s00382-011-1159-1.

Kilonsky, B. J., and C. S. Ramage, 1976: A technique for estimating tropical open-ocean rainfall from satellite observations. *J. Appl. Meteor.*, **15**, 972–975, doi:10.1175/1520-0450(1976)015<0972:ATFETO>2.0.CO;2.

Konwar, M., S. K. Das, S. M. Deshpande, K. Chakravarty, and B. N. Goswami, 2014: Microphysics of clouds and rain over the Western Ghat. *J. Geophys. Res. Atmos.*, **119**, 6140–6159, doi:10.1002/2014JD021606.

Krishnamurti, T. N., S. Cocke, R. Pasch, and S. Low-Nam, 1983: Precipitation estimates from raingauge and satellite observations: Summer MONEX. Dept. of Meteorology, Florida State University, 373 pp.

Kumar, S., A. Hazra, and B. N. Goswami, 2014: Role of interaction between dynamics, thermodynamics and cloud microphysics on summer monsoon precipitating clouds over the Myanmar coast and the Western Ghats. *Climate Dyn.*, **43**, 911–924, doi:10.1007/s00382-013-1909-3.

Kummerow, C., D. L. Randel, M. Kulie, N.-Y. Wang, R. Ferraro, S. J. Munchak, and V. Petkovic, 2015: The evolution of the Goddard profiling algorithm to a fully parametric scheme. *J. Atmos. Oceanic Technol.*, **32**, 2265–2280, doi:10.1175/JTECH-D-15-0039.1.

Liebmann, B., and C. A. Smith, 1996: Description of a complete (interpolated) outgoing longwave radiation dataset. *Bull. Amer. Meteor. Soc.*, **77**, 1275–1277.

Lin, Y.-L., 2007: *Mesoscale Dynamics.* Cambridge University Press, 630 pp.

Mori, S., and Coauthors, 2004: Diurnal land–sea rainfall peak migration over Sumatera Island, Indonesian Maritime Continent, observed by TRMM satellite and intensive rawinsonde soundings. *Mon. Wea. Rev.*, **132**, 2021–2039, doi:10.1175/1520-0493(2004)132<2021:DLRPMO>2.0.CO;2.

Nugent, A. D., R. B. Smith, and J. R. Minder, 2014: Wind speed control on tropical orographic convection. *J. Atmos. Sci.*, **71**, 2695–2712, doi:10.1175/JAS-D-13-0399.1.

Ogino, S.-Y., M. D. Yamanaka, S. Mori, and J. Matsumoto, 2016: How much is the precipitation amount over the tropical coastal region? *J. Climate*, **29**, 1231–1236, doi:10.1175/JCLI-D-15-0484.1.

Ogura, Y., and M. Yoshizaki, 1988: Numerical study of orographic-convective precipitation over the eastern Arabian Sea and the Ghat Mountains during the summer monsoon. *J. Atmos. Sci.*, **45**, 2097–2122, doi:10.1175/1520-0469(1988)045<2097:NSOOCP>2.0.CO;2.

Peatman, S. C., A. J. Matthews, and D. P. Stevens, 2014: Propagation of the Madden–Julian Oscillation through the Maritime Continent and scale interaction with the diurnal cycle of precipitation. *Quart. J. Roy. Meteor. Soc.*, **140**, 814–825, doi:10.1002/qj.2161.

Rauniyar, S. P., and K. J. E. Walsh, 2011: Scale interaction of the diurnal cycle of rainfall over the Maritime Continent and Australia: Influence of the MJO. *J. Climate*, **24**, 325–348, doi:10.1175/2010JCLI3673.1.

Rickenbach, T. M., 1999: Cloud top evolution of tropical oceanic squall lines from radar reflectivity and infrared satellite data. *Mon. Wea. Rev.*, **127**, 2951–2976, doi:10.1175/1520-0493(1999)127<2951:CTEOTO>2.0.CO;2.

Romatschke, U., and R. A. Houze Jr., 2011: Characteristics of precipitating convective systems in the South Asian monsoon. *J. Hydrometeor.*, **12**, 3–26, doi:10.1175/2010JHM1289.1.

Shige, S., and C. D. Kummerow, 2016: Precipitation-top heights of heavy orographic rainfall in the Asian monsoon region. *J. Atmos. Sci.*, **73**, 3009–3024, doi:10.1175/JAS-D-15-0271.1.

——, S. Kida, H. Ashiwake, T. Kubota, and K. Aonashi, 2013: Improvement of TMI rain retrievals in mountainous areas. *J. Appl. Meteor. Climatol.*, **52**, 242–254, doi:10.1175/JAMC-D-12-074.1.

——, M. K. Yamamoto, and A. Taniguchi, 2015: Improvement of TMI rain retrieval over the Indian subcontinent. *Remote Sensing of the Terrestrial Water Cycle*, *Geophys. Monogr.*, Vol. 206, Amer. Geophys. Union, 27–42, doi:10.1002/9781118872086.ch2.

Slingo, J., P. Inness, R. Neale, S. Woolnough, and G.-Y. Yang, 2003: Scale interactions on diurnal to seasonal timescales and their relevance to model systematic errors. *Ann. Geophys.*, **46**, 139–155.

Smith, R. B., and Y.-L. Lin, 1983: Orographic rain on the Western Ghats. *Mountain Meteorology*, E. R. Reiter et al., Eds., Science Press and Amer. Meteor. Soc., 71–94.

Sui, C.-H., and K.-M. Lau, 1992: Multiscale phenomena in the tropical atmosphere over the western Pacific. *Mon. Wea. Rev.*, **120**, 407–430, doi:10.1175/1520-0493(1992)120<0407:MPITTA>2.0.CO;2.

Taniguchi, A., and Coauthors, 2013: Improvement of high-resolution satellite rainfall product for Typhoon Morakot (2009) over Taiwan. *J. Hydrometeor.*, **14**, 1859–1871, doi:10.1175/JHM-D-13-047.1.

Tian, B., D. E. Waliser, and E. J. Fetzer, 2006: Modulation of the diurnal cycle of tropical deep convective clouds by the MJO. *Geophys. Res. Lett.*, **33**, L20704, doi:10.1029/2006GL027752.

Wang, B., P. Webster, K. Kikuchi, T. Yasunari, and Y. J. Qi, 2006: Boreal summer quasi-monthly oscillation in the global tropics. *Climate Dyn.*, **27**, 661–675, doi:10.1007/s00382-006-0163-3.

Webster, P. J., V. O. Magana, T. N. Palmer, J. Shukla, R. A. Tomas, M. Yanai, and T. Yasunari, 1998: Monsoons: Processes, predictability, and the prospects for prediction. *J. Geophys. Res.*, **103**, 14 451–14 510, doi:10.1029/97JC02719.

Williams, M., and R. A. Houze Jr., 1987: Satellite-observed characteristics of winter monsoon cloud clusters. *Mon. Wea. Rev.*, **115**, 505–519, doi:10.1175/1520-0493(1987)115<0505:SOCOWM>2.0.CO;2.

Wu, P., M. Hara, J. Hamada, M. D. Yamanaka, and F. Kimura, 2009: Why a large amount of rain falls over the sea in the vicinity of western Sumatra Island during nighttime. *J. Appl. Meteor. Climatol.*, **48**, 1345–1361, doi:10.1175/2009JAMC2052.1.

Xie, S.-P., H. M. Xu, N. H. Saji, Y. Q. Wang, and W. T. Liu, 2006: Role of narrow mountains in large-scale organization of Asian monsoon convection. *J. Climate*, **19**, 3420–3429, doi:10.1175/JCLI3777.1.

Yamamoto, M. K., and S. Shige, 2015: Implementation of an orographic/nonorographic rainfall classification scheme in the

GSMaP algorithm for microwave radiometers. *Atmos. Res.*, **163**, 36–47, doi:10.1016/j.atmosres.2014.07.024.

——, ——, C.-K. Yu, and L.-W. Chen, 2017: Further improvement of the heavy orographic rainfall retrievals in the GSMaP algorithm for microwave radiometers. *J. Appl. Meteor. Climatol.*, **56**, 2607–2619, doi:10.1175/JAMC-D-16-0332.1.

Yamanaka, M. D., 2016: Physical climatology of Indonesian Maritime Continent: An outline to comprehend observational studies. *Atmos. Res.*, **178–179**, 231–259, doi:10.1016/j.atmosres.2016.03.017.

Yasunari, T., 1979: Cloudiness fluctuations associated with the Northern Hemisphere summer monsoon. *J. Meteor. Soc. Japan*, **57**, 227–242, doi:10.2151/jmsj1965.57.3_227.

Yokoi, S., and T. Satomura, 2008: Geographical distribution of variance of intraseasonal variations in western Indochina as revealed from radar reflectivity data. *J. Climate*, **21**, 5154–5161, doi:10.1175/2008JCLI2153.1.